PCCP

State specific dynamics of the $H^- + H_2 \rightarrow H_2 + H^-$ reaction: Energy resolved total reaction probabilities by the time-dependent wave packet method

Susanta Mahapatra*†

Department of Chemistry, Indian Institute of Technology, Kanpur, 208 016, India

Received 16th September 1999, Accepted 12th November 1999

Reagent ro-vibrational state-selected and energy resolved total reaction probabilities of the title reaction are calculated on the diatomics-in-molecules potential energy surface of Belyaev *et al.* (*Chem. Phys.*, 1997, **220**, 43). A three dimensional time-dependent wave packet (WP) method for the total angular momentum $J = 0$ is employed for the purpose. The reaction probabilities are obtained by the time–energy mapping of the reactive flux of the WP across a dividing surface in the asymptotic product channel. While the initial vibrational excitation of reagent H_2 is shown, in general, to decrease the reaction probability at low and moderate energies, the initial rotational excitation does not lead to any such general trend. Existence of resonances is indicated in the reaction with ro-vibrationally hot H_2 molecules. The energetic threshold and other dynamical features of the reaction are in accord with the experimental findings.

I. Introduction

The reaction

$$H^- + H_2 \rightarrow H_2 + H^-, \qquad \text{(R1)}$$

is perhaps the simplest example of an S_N2 type of chemical reaction with closed shell reactants. It belongs to the family of fundamental hydrogen exchange reactions. The neutral reactive system of this family

$$H + H_2 \rightarrow H_2 + H, \qquad \text{(R2)}$$

has been extensively studied both experimentally and theoretically over the past few decades (for example, see ref. 1). It has served as a benchmark system in the study of reactive scattering dynamics. With the advent of improved quantum chemical methods it has been possible to calculate accurate potential energy surfaces[2] for this system which in turn has enabled one to complement the experimental results on H_3 and its isotopic variants in the theoretical studies.[3,4] On the other hand, to date, very little is known on the reactive scattering dynamics of (R1). Although the stability of H_3^- was predicted long ago,[5] the reaction (R1) has drawn the attention of researchers only recently. Qualitatively, the reaction (R1) has much similarity with (R2) in the sense that both proceed through a barrier of nearly equal height. However, the extra electron in (R1) leads to a new reaction channel, *viz*. the electron detachment channel. This opens up new mechanistic pathways which are important mechanisms in hydrogen discharges and H^- sources. Furthermore, collision dynamics involving negative ions is an open and interesting field of research. At large H^-–H_2 distances, the charge-induced dipole interaction leads to a local minimum in its potential energy surface (PES). Therefore, the microscopic details of the dynamics of (R1) are expected to be considerably different from that of (R2) and an elaborate study (both experimental and theoretical) on (R1) would be valuable in improving our understanding of the dynamics of this prototypical system involving negative ions.

Earlier theoretical studies on (R1) focussed mainly on the stability of H_3^-.[6–9] On the experimental front, early effort was devoted to a measurement of the elastic and inelastic scattering cross sections in H^-–H_2 collisions.[10,11] Michaels and Paulson[7] had first measured the cross sections for the $H^- + D_2$ and $D^- + H_2$ exchange reactions. The electron detachment cross sections were measured by Haq *et al.*[12] Subsequently, measurements by Zimmer and Linder[13] provided new experimental data on the reactive process (R1) and

$$H^- + D_2 \rightarrow HD + D^-. \qquad \text{(R3)}$$

In addition, they also measured the vibrational and rotational inelasticity in $H^- + H_2$ collisions.[11] Haufler *et al.*[14] have recently measured the absolute differential and integral cross sections for (R3) and

$$D^- + H_2 \rightarrow H^- + HD \qquad \text{(R4)}$$

reactions in a guided ion beam apparatus.

Until recently, the theoretical description of (R1) and its isotopic variants was handicapped by the absence of a three-dimensional PES. The *ab initio* computations are known to be prohibitively difficult for quasi-bound molecular anions. Three-dimensional diatomics-in-molecules (DIM) potential energy surfaces for the ground and a few low-lying excited states were reported by Belyaev *et al.*[15] These potential energy surfaces have subsequently been improved by Belyaev and Tiukanov[16] over the full range of geometrical configurations of H_3^-. Their study also revealed that the ground and first excited states of H_3^- are orbitally degenerate at the D_{3h} symmetry configuration and that they form a conical intersection. An analytical *ab initio* PES for the ground electronic state of H_3^- was reported by Stärck and Meyer.[17] Both the DIM[15,16] and the Stärck–Meyer (SM)[17] PESs for the ground electronic state of H_3^- revealed the existence of a saddle point for the collinear arrangement of the three H nuclei. The crest of the barrier is found at $r_{H^- - H} = r_{H-H} = 1.74\ a_0$‡ on the DIM

† Present address: Theoretical Chemistry, Physical Chemistry Institute, University of Heidelberg, Im Neuenheimer Feld 229, D-69120 Heidelberg, Germany.

‡ $1\ a_0 = 5.291\,77 \times 10^{-11}$ m.

PES[15,16] and at 1.997 a_0 on the SM PES.[17] The height of the barrier is 0.624 eV on the DIM and 0.457 eV on the SM PES, respectively. Both the DIM and SM potential energy surfaces exhibit a shallow van der Waals well of depth $\approx$0.05 eV for the collinear arrangement of the nuclei at $R \approx 6\ a_0$ (where R denotes the distance of the third H atom from the center-of-mass of the other two).

It is reported that the ground electronic PES of H_3^- crosses the ground electronic PES of H_3 at small internuclear distances.[8,17] This is supposed to lead to the electron detachment. The minimum of the electron detachment seam has been found at $R = 2.87\ a_0$, $r = 1.42\ a_0$ at the C_{2v} arrangements of H_3^- with an energy of 1.2 eV on the SM PES.[17] An alternative mechanism for the electron detachment process is proposed by Belyaev *et al.*[16] The ground electronic state of H_3 lies above that of H_3^-. During collisions H_3^- could undergo a transition to its first excited electronic state which is nonadiabatically coupled to its ground electronic state.[16] H_3^- is quasi-stationary in the first excited electronic state and can decay to the ground electronic state of H_3 by emitting a free electron. An energetic threshold value of 1.46 eV for the electron detachment in H^-–H_2 collisions is estimated on the DIM PES.[16] An experimental value of 1.45 $\pm$ 0.1 eV has been reported for this quantity.[12] A correct description of this electron detachment channel in a theoretical study involves treatment of nuclear dynamics simultaneously on more than one electronic potential energy surface. This is an elaborate task and due to the lack of sufficient informations on the participating electronic states and their coupling elements we neglect this channel in the following dynamical study.

Belyaev *et al.*[15] have carried out state-to-state reaction probability calculations for (R1) and (R3) for the collinear configuration on the DIM PES by the *S*-matrix Kohn variational method in the discrete variable representation (DVR). The reaction thresholds obtained by them are in good agreement with the experimental results.[13] Mahapatra and Sathyamurthy have reported the initial state selected and energy resolved total reaction probabilities for (R1) on the SM PES both for the collinear[18] and three dimensional[19] arrangements of the nuclei using the time-dependent wave packet (WP) propagation method. Their results indicated the existence of resonances on the SM PES which are not found in the calculations of Belyaev *et al.*[15] on the DIM PES. Mahapatra *et al.*[20] have also analyzed and characterized some of these collinear resonances by the spectral quantization approach. Ansari and Sathyamurthy[21] have carried out quasiclassical trajectory studies on the SM PES for the collinear arrangement and obtained total reaction probabilities in agreement with the time-dependent WP results.[18] They have also analyzed the phase space behavior of trajectories in terms of action-angle and Poincaré surface-of-section plots and pointed out the existence of both regular and irregular type of trajectories in collinear H_3^-.[21] Dynamical calculations on the vibrational and rotational inelasticity on the SM PES are reported by Gianturco and Kumar.[22]

Despite the aforementioned studies, a detailed theoretical understanding of the dynamics of the reaction (R1) and its isotopic variants is still missing. The theoretical description of the nuclear dynamics is limited by the accuracy of the available electronic PES for the system.

In this paper we report on the reagent state selected and energy resolved reaction probabilities for (R1) in three dimensions on the DIM PES using a time-dependent WP approach. In the following we focus only on the ground electronic PES of the system. The coupling to the first excited state and the impact of the conical intersection on the reactive scattering dynamics of this system will be treated in a separate article. The dynamical results are found to be consistent with the experimentally observed behavior of the system. The results obtained on the SM PES in our previous work[19] are also compared with the present results in order to shed light on the sensitivity of the dynamics to the available potential energy surfaces of this prototypical system.

The paper is organized in the following way. In section II we outline the theoretical approach, and the results obtained are presented and discussed in section III. The paper is closed with a succinct summary in section IV.

II. Theoretical framework to treat the reactive scattering dynamics

The three-dimensional (3D) interaction Hamiltonian for the A + BC collisional system in mass-scaled reactant channel Jacobi coordinates (R, r, γ) and for the total angular momentum $J = 0$ in the body-fixed frame is given by[23]

$$\begin{aligned}\hat{H} &= \frac{1}{2\mu}[P_R^2 + P_r^2] + \frac{\boldsymbol{j}^2}{2I} + V(R, r, \gamma) \\ &= -\frac{\hbar^2}{2\mu}\left[\frac{\partial^2}{\partial R^2} + \frac{\partial^2}{\partial r^2}\right] \\ &\quad -\frac{\hbar^2}{2I}\frac{1}{\sin\gamma}\frac{\partial}{\partial\gamma}\left(\sin\gamma\,\frac{\partial}{\partial\gamma}\right) + V(R, r, \gamma), \end{aligned} \tag{1}$$

where P_R and P_r are the momentum operators corresponding to the two mass-scaled Jacobi distances R (distance of atom A from the center of mass of the BC molecule) and r (BC internuclear distance), respectively, and $\boldsymbol{j}$ is the rotational angular momentum operator of the BC molecule. The quantity μ [$= \sqrt{m_A m_B m_C/(m_A + m_B + m_C)}$, where m_A, m_B and m_C are the masses of the nuclei A, B and C, respectively] is the three-body reduced mass, and I [$=\mu R^2 r^2/(R^2 + r^2)$] is the moment of inertia of the system. The body-fixed z axis is taken to be parallel to the Jacobi vector $\boldsymbol{R}$ and BC lies in the (x, z) plane. The DIM PES for the ground electronic state of H_3^- is employed for $V(R,r,\gamma)$.[15,16]

The dynamics of the system is followed by numerically solving the time-dependent Schrödinger equation (TDSE) on a grid in (R, r, γ) space. For an explicitly time-independent Hamiltonian, the solution reads

$$\Psi(t) = \exp\left[\frac{-i\hat{H}t}{\hbar}\right]\Psi(t = 0). \tag{2}$$

Here $\Psi(t = 0)$ is the initial wavefunction pertinent to the reactants and $\Psi(t)$ is the wavefunction at time t. Once the TDSE is solved, the energy resolved reaction probability $P_{vj}^R(E)$ [where the suffix vj denotes the initial vibrational (v) and rotational (j) states of the BC molecule] is obtained from[24–27]

$$P_{vj}^R(E) = \frac{\hbar}{\mu}\,\mathrm{Im}\left[\left\langle\left\langle \Psi(R, r_I, \gamma, E)\left|\frac{\partial\Phi(R, r_I, \gamma, E)}{\partial r}\right\rangle\right\rangle\right], \tag{3}$$

where the quantity within angular brackets ($\langle\langle\ \rangle\rangle$) is the energy resolved flux of the WP across a dividing surface at $r = r_I$. The integration (represented by $\langle\langle\ \rangle\rangle$) is carried out over the entire range of R and γ. The quantity E represents the total (relative translational plus the BC ro-vibrational energy) energy of the collisional system. $\Phi(R, r_I, \gamma, E)$ is the energy resolved wavefunction normalised with respect to the initial translational energy distribution of the WP and calculated along the dividing surface at $r = r_I$:

$$\Phi(R, r_I, \gamma, E) = \psi(R, r_I, \gamma, E)/\kappa_E. \tag{4}$$

The function $\psi(R, r_I, \gamma, E)$ is obtained by Fourier transforming the time evolved WP $\Psi(R, r, \gamma, t)$ along the dividing surface:

$$\psi(R, r_I, \gamma, E) = \frac{1}{\sqrt{2\pi}}\int_{-\infty}^{+\infty}\Psi(R, r, \gamma, t)e^{iEt/\hbar}\,dt\Big|_{r=r_I}. \tag{5}$$

The quantity κ_E in eqn. (4) is the weight of the translational

Table 1 Numerical grid parameters and properties of the initial wavefunction used in the calculations of reaction probabilities

Parameters		
$N_R/N_r/N_\gamma$	128/128/29	Number of grid points
R_{min}/R_{max} (a_0)	0.80/16.04	Extension of the grid along R
r_{min}/r_{max} (a_0)	0.50/15.74	Extension of the grid along r
$\Delta R = \Delta r$ (a_0)	0.12	Grid spacings along R and r
r_I (a_0)	4.1	Location of the dividing surface in the product channel
R_{mask}/r_{mask} (a_0)	12.36/5.16	Starting point of the masking function
R_0 (a_0)	10.5	Initial location of the center of the GWP in the coordinate space
κ_0 (au[a])	9.79	Initial location of the center of the GWP in the momentum space
δ (a_0)	0.25	Initial width parameter of the GWP
Δt (fs)	0.1347	Length of the time step used in the WP propagation
T (fs)	413.76	Total propagation time

[a] Here, 1 au = 2.19474×10^3 m^{-1}.

energy component contained in the initial WP for a given total energy E:

$$\kappa_E = \left(\frac{\mu}{2\pi\hbar k}\right)^{1/2} \int_{-\infty}^{+\infty} F(R) e^{ikR}\, dR, \tag{6}$$

where $F(R)$ is the translational component of the initial WP and $k = \sqrt{2\mu(E - \varepsilon_{vj})}/\hbar$, with ε_{vj} being the ro-vibrational energy of the BC molecule.

The action of the time evolution operator $\exp[-i\hat{H}t/\hbar]$ on the wavefunction in eqn. (2) is carried out by dividing the total time into N segments of length Δt each. The exponential operator at each time step is then approximated by the split-operator (SO) method:[28]

$$\exp\left[\frac{-i\hat{H}\Delta t}{\hbar}\right] = \exp\left[\frac{-iV\Delta t}{2\hbar}\right]\exp\left[\frac{-ij^2\Delta t}{4I\hbar}\right] \times \exp\left[\frac{-iT\Delta t}{\hbar}\right]\exp\left[\frac{-ij^2\Delta t}{4I\hbar}\right] \times \left[\frac{-iV\Delta t}{2\hbar}\right] + O[(\Delta t)^3] \tag{7}$$

where $T = (P_R^2 + P_r^2)/2\mu$, is the total radial kinetic energy operator. The above equation is used in conjunction with the fast Fourier transform (FFT) method[29] to evaluate the action of the exponential containing the radial kinetic energy operator and the DVR method[30–33] to evaluate the exponential containing the rotational kinetic energy operator ($j^2/2I$) on the wavefunction. The latter is carried out by transforming the grid wave function to the angular momentum space (finite basis representation, FBR), multiplying it by the diagonal value of the operator ($e^{-ij(j+1)\Delta t\hbar/4I}$), and transforming it back to the grid representation (DVR). Numerically this is accomplished in a single step:[33]

$$\exp\left[\frac{-ij^2\Delta t}{4I\hbar}\right]\Psi_{lmn'} = \sum_n \left\{\sum_j \boldsymbol{T}^{\dagger}_{n',j}\, e^{-ij(j+1)\Delta t\hbar/4I} \boldsymbol{T}_{j,n}\right\}\Psi_{lmn}, \tag{8}$$

where j is the rotational quantum number of BC. The coefficients $\boldsymbol{T}_{j,n}$ are the elements of the DVR-FBR transformation matrix, constructed in terms of Legendre polynomials (eigenfunctions of the j^2 operator):[30–33]

$$\boldsymbol{T}_{j,n} = \sqrt{w(n)}\sqrt{\frac{2j+1}{2}} P_j(\cos\gamma_n), \tag{9}$$

and $\boldsymbol{T}^{\dagger}_{n,j}$ are the elements of the inverse transformation matrix, the Hermitian conjugate to $\boldsymbol{T}_{j,n}$.

In the scattering studies the initial WP, $\Psi(0)$, is prepared in the asymptotic reactant channel, where practically there is no influence of the interaction potential. In such a situation it can be written as a direct product of the (A, BC) translational wavefunction and the ro-vibrational eigenfunction of the BC molecule. In the present case, for $J = 0$, it is given by

$$\Psi(R, r, \gamma, t = 0) = F(R)\phi_{vj}(r)\sqrt{\frac{2j+1}{2}} P_j(\cos\gamma), \tag{10}$$

where $F(R)$ is a minimum uncertainty Gaussian wave packet (GWP) corresponding to the (A, BC) translational motion:

$$F(R) = \left(\frac{1}{2\pi\delta^2}\right)^{1/4} \exp\left[-\frac{(R - R_0)^2}{4\delta^2} - ik_0 R\right]. \tag{11}$$

The quantity δ is the width parameter of the GWP and R_0 and k_0 correspond to the location of its maximum in the coordinate and momentum space, respectively. The function $\phi_{vj}(r)$ along with the normalized Legendre polynomials represents the ro-vibrational eigenfunction corresponding to the (v, j) state of the BC molecule. The function $\phi_{vj}(r)$ is obtained by solving the eigenvalue equation of the free BC molecule:

$$\left[-\frac{\hbar^2}{2\mu'}\frac{d^2}{dr'^2} + V(r') + \frac{j(j+1)\hbar^2}{2\mu' r'^2}\right]\phi_{vj}(r') = \varepsilon_{vj}\phi_{vj}(r'). \tag{12}$$

Here μ' is the reduced mass of BC, ε_{vj} the energy eigenvalue, $r'[=r(\mu/\mu')^{1/2}]$ the unscaled internuclear distance, and $V(r')$ is the potential energy of the free BC molecule obtained from the DIM PES by setting $R \to \infty$. In the following we employ the sine-DVR approach of Colbert and Miller[34] to solve the above eigenvalue equation.

The dynamical calculations were carried out on a grid consisting of equally spaced points R_l and r_m along the Jacobi distances R and r, respectively. The grid along the Jacobi angle γ is chosen as the nodes of a n-point Gauss–Legendre quadrature (GLQ).[35] The initial WP at each node (R_l, r_m, γ_n) of this grid is given by:

$$\Psi(R_l, r_m, \gamma_n, t = 0) = \Psi_{lmn} = \sqrt{w_n}\, F(R_l)\phi_{vj}(r_m)\sqrt{\frac{2j+1}{2}} P_j(\cos\gamma_n) \tag{13}$$

where w_n is the weight of the GLQ associated with the grid point n.

In dynamical studies involving scattering systems, as the WP moves forward in time, its fast moving components approach the grid boundaries and are no longer relevant for the rest of the dynamics.[24] Therefore, to avoid unphysical reflections or wrap arounds of these components from the boundaries of a finite sized grid, the WP at each time step is multiplied by a damping function[36]

$$f(X_i) = \sin\left[\frac{\pi}{2}\frac{(X_{mask} + \Delta X_{mask} - X_i}{\Delta X_{mask}}\right], \quad X_i \geqslant X_{mask} \tag{14}$$

which is activated outside the dividing line in the product channel and also in the asymptotic reactant channel. X_{mask} is the point at which the damping function is initiated and $\Delta X_{mask}(= X_{max} - X_{mask})$ is the width of X over which the

function decays from 1 to 0, with X_{max} being the maximum value of X in that direction, in a particular channel. The properties of the initial WP and the grid parameters used for the numerical calculations are listed in Table 1.

III. Results and discussion

In this section we present the reaction probabilities of (R1) obtained from the flux formula in eqn. (3) for various initial ro-vibrational states of the reagent H_2. The reaction probabilities are calculated at an energy interval of 5×10^{-3} eV. The convergence of the results is checked explicitly for different choices of parameters used in the numerical calculations.

The energy resolved reaction probabilities of (R1), for H_2 initially in the $v = 0$ and $j = 0$–3 states, are plotted as a function of E in Fig. 1. The reaction probability curves for $j = 0$, 1, 2 and 3 are shown in the figure by the full, dashed, long-dashed and dot-dashed lines, respectively. The energy E is measured from the minimum of the H_2 potential. The reaction probabilities are summed over all open vibrational (v') and rotational (j') channels of the product H_2 at a given energy E, and therefore, they represent the total reaction probabilities. It can be seen from the figure that the reaction starts at $E = 0.62$ eV and the reaction probability increases rapidly with energy, reaches a maximum value and again falls off at higher energies. This energy threshold of 0.62 eV represents the barrier to the hydrogen exchange on the DIM PES.[15] The experimental threshold for (R1) is unknown, but the calculated results can be compared with the experimental results for (R3) and with other calculations for (R1). The experimentally recorded energetic threshold for the reaction (R3) is reported at 0.42 ± 0.12 eV[13] and at 0.35 ± 0.06 eV.[14] These energetic thresholds correspond to the above barrier height reduced by the initial vib-rotational ($v = 0$, $j = 0$) energy of the reagent molecule. The vib-rotational energy of D_2 ($v = 0$, $j = 0$) is 0.19 eV. Therefore, the energetic threshold for (R3) on the DIM PES occurs at $\sim$0.41 eV, which is in good agreement with the experimental value within the uncertainties. The height of the reaction barrier is found to be unchanged by the isotopic substitution (within the Born–Oppenheimer approximation). However, the energetic threshold changes due to a change in the zero-point energy of the reacting system. The ro-vibrational energy of H_2 ($v = 0$, $j = 0$) is 0.27 eV, and therefore, the threshold for (R1) occurs at $\sim$0.35 eV on the DIM PES. An energetic threshold of 0.49 eV for (R3) was estimated by Stärk and Meyer.[17] They obtained this value from the curvature of their *ab initio* PES at the H_3^- transition state which actually represents the threshold including the zero-point energy; and was not the result of a scattering calculation. We performed quantum scattering studies on the SM PES and found the energetic threshold at $\sim$0.32 eV for (R1) and $\sim$0.39 eV for (R3),[19] in close agreement with the experimental results.[13,14]

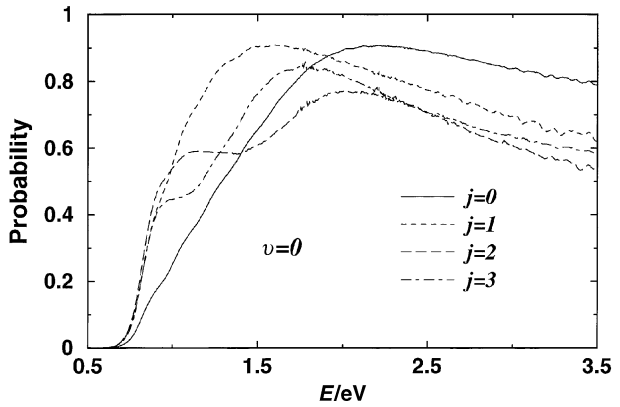

Fig. 1 Total reaction probability as a function of the total energy $E(H^-, H_2$ translational + H_2 ro-vibrational) for the $H^- + H_2(v = 0, j = 0\text{–}3) \rightarrow H_2(\Sigma v', \Sigma j') + H^-$ exchange reaction on the DIM PES in three-dimensions, for total angular momentum $J = 0$. The energy E is measured from the minimum of the H_2 potential. Reaction probability curves for $j = 0$, 1, 2 and 3 are indicated in the panel by the solid, dashed, long-dashed and dot-dashed lines, respectively.

The reaction probability curve for H_2 ($v = 0, j = 0$) in Fig. 1 shows a broad maximum around $\sim$2 eV and this maximum shifts to a lower energy on rotational excitation of H_2. The initial state selected ($v = 0$, $j = 0$) total cross sections of (R3) measured by Zimmer and Linder[13] also show a similar variation with energy. The reaction cross section starting from the threshold at $\sim$0.42 eV rises to a maximum at $\sim$1.5 eV and then decreases rapidly at higher energies.[13] A quantitative comparison with the experiment can be made only when the other energetically allowed processes are included in the theoretical treatment and also the treatment is extended to $J \neq 0$ collisions to calculate the reaction cross sections. Such a study is presently being taken up. The reaction probability of rotationally excited H_2 increases much more rapidly at the onset of the reaction and also falls off more rapidly at higher energies. Interestingly, all $j \neq 0$ probability curves show a similar increase of the reaction probability at the onset, and therefore, the rotationally excited H_2 increases the reactivity to the same extent at low energies. The probability curves for $j = 2$ and 3 exhibit bimodal distributions indicating the appearance of a broad resonance in reaction with rotationally hot H_2. This resonance structure shifts down to a lower energy for $j = 3$.

Since the potential energy surfaces of (R1) and (R2) are qualitatively similar, at this point it is worthwhile to compare the above dynamical results with those reported for (R2). The initial state-selected and energy resolved total reaction probabilities of (R2) have been reported by several groups.[37–39] The barrier for the exchange reaction (R2) is also minimum for the collinear approach of the nuclei. The reported magnitude of the height of the classical barrier for (R2) is $\sim$0.42 eV, occurring for the collinear arrangement of the nuclei at $r_{H-H} \approx 1.76\ \alpha_0$.[2] The onset of the reaction (R2) is found at $E = 0.55$ eV for $H_2(v = 0,\ j = 0)$.[37–39] Therefore, both (R1) and (R2) have nearly identical reaction thresholds. In contrast to that of (R1) the reaction probability curves of (R2) reveal many resonance structures. The overall variation of the reaction probability with energy for rotationally excited H_2 molecules is similar for both (R1) and (R2) [for example, see a similar drawing as in Fig. 1 presented in Fig. 3 of ref. 39 for (R2)].

The reaction probability curves of (R1) for H_2 initially in the $v = 1$ and $j = 0$–3 states are shown in Fig. 2. As for $v = 0$, the probability curves for $j = 0$, 1, 2 and 3 are shown in the panel by the solid, dashed, long-dashed and dot-dashed lines, respectively. The overall variation of reaction probabilities for different rotational states of H_2 is similar to that observed in Fig. 1. However, with reagent vibrational excitation the reaction threshold shifts to a higher energy. It can be seen that the barrier to the reaction for $v = 1$ and $j = 0$ is $\sim$0.95 eV. This amounts to a shift of $\sim$0.33 eV from the threshold for the

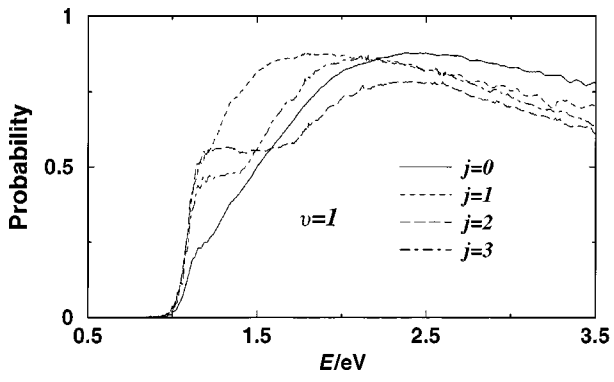

Fig. 2 Same as in Fig. 1 for $H^- + H_2(v = 2,\ j = 0\text{–}3) \rightarrow H_2(\Sigma v', \Sigma j') + H^-$ exchange reaction.

reaction for $v = 0$, $j = 0$. The vibrational energy of $H_2(v = 1, j = 0)$ is 0.785 eV. Therefore, only a part of this vibrational quantum is utilized in overcoming the barrier. With the reagent vibrational excitation the probability maximum shifts to a higher energy. Moreover, a decrease in the reaction probability at low and moderate energies can be seen from the solid curve of Fig. 2, when compared to the probability curve for H_2 ($v = 0, j = 0$) of Fig. 1. The reagent vibrational excitation, therefore, decreases reactivity at low and moderate energies. This means that at low and moderate energies reagent translational energy is more efficient in promoting the reaction. At high energies the probability curve for $v = 1$, $j = 0$ coincides with that for $v = 0$, $j = 0$. A similar interplay between the reagent translational–vibrational energies in promoting the reaction at low energies has been noted in $H + D_2$ collisions.[40] In addition, it can be seen from Fig. 2 that the resonance structures become more prominent in the probability curves of the ro-vibrationally excited H_2 molecule.

In order to clearly reveal these resonances the reaction probability curves of (R1) for $H_2(v = 2, j = 0–3)$ are plotted in four separate panels in Fig. 3. The onset of the reaction for $v = 2$ again shifts by $\sim$0.33 eV to a higher energy compared to that for $v = 1$. The reaction probability maximum shifts further to a higher energy from that for $v = 1$, $j = 0$, and also a further decrease in the reaction probability at low and moderate energies can be noticed from Fig. 3. Therefore, the reagent vibrational excitation, in general, decreases the reactivity at low and moderate energies. Again, the overall reactivity for different j states of H_2 exhibits a similar pattern as observed in Fig. 1 and 2. The most interesting aspects of the reaction with ro-vibrationally hot reagent H_2 molecule is the appearance of sharp resonance structures at the onset of the reaction. It would be gratifying to see these resonances in an experimental recording which would test the quality of the potential energy surface of this seemingly simple prototypical reactive system.

At this point it is worthwhile to compare the shift of the energy onset of the reaction (R1) from $v = 0$ to $v = 1$ to $v = 2$ with the vibrationally adiabatic barriers between the reactant and the transition state (TS). The zero-point energy of the TS estimated from the *ab initio* vibrational frequencies[17] is $\sim$0.45 eV. The energy barrier on the DIM PES is 0.62 eV and the zero-point energy of H_2 molecule is 0.27 eV. Therefore, the vibrationally adiabatic barrier for $v = 0$ is $\sim$0.80 eV. This barrier shifts to the higher energy by an amount $\sim$0.40 eV from $v = 0$ to $v = 1$ and from $v = 1$ to $v = 2$. As noted above, the onset of the reaction shifts by an amount $\sim$0.33 eV in that order.

We now compare the results obtained on the DIM PES with those obtained on the SM PES in our earlier work.[18,19] The reaction probabilities of (R1) obtained for both the collinear and the three-dimensional ($J = 0$) arrangements of the nuclei are plotted as a function of the total energy E in Fig. 4(a and b), respectively. The above reaction probabilities correspond to the reaction with the H_2 molecule initially in its vibrational and rotational ground state ($v = 0$, $j = 0$). The probabilities are summed over all open internal channels of the product H_2. The grid parameters and other computational details are identical to those mentioned above. The results obtained on the SM and DIM potential energy surfaces are indicated by the solid and dashed lines, respectively, in both Fig. 4(a) and 4(b). Although the reaction (R1) is dominated by the collinear configuration (which is true only in the vicinity of the reaction threshold) a substantial impact of the angular degree of freedom can be found on moving from the collinear [Fig. 4(a)] to the three-dimensional [Fig. 4(b)] results. The resonance structures seen in the collinear results almost disappear in the three-dimensional ones. It can be seen from both Fig. 4(a) and 4(b) that the reaction (R1) has a lower threshold on the SM PES and the probability maximum occurs at a lower energy on this PES. Despite this, the overall qualitative energy dependence of the collinear reaction probabilities for both surfaces is quite similar. The oscillations in both collinear and three-dimensional reaction probability curves obtained on the SM PES are absent in those obtained on the DIM PES. This highlights the sensitivity of the dynamics to the microscopic details of the potential energy surfaces. It is to be noted here that the convergence behavior of the reaction probability on the SM PES depends significantly on the location of the dividing surface in the product channel. The above results are obtained by calculating the reactive flux along a dividing surface at $r_I = 3.02\ \alpha_0$ on both SM and DIM potential energy surfaces.

The SM PES is the only three-dimensional *ab initio* PES available for this system and it is expected to be more accurate than the DIM PES. As discussed in the previous paragraphs, the dynamical features of (R1) on the DIM PES correspond well with the experimental behavior as well as

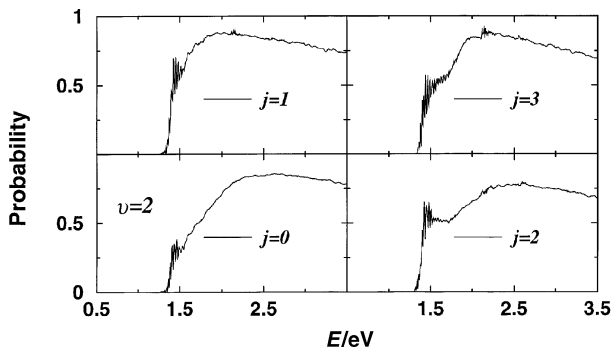

Fig. 3 Same as in Fig. 1 for $H^- + H_2(v = 1, j = 0–3) \rightarrow H_2(\Sigma v', \Sigma j') + H^-$ exchange reaction.

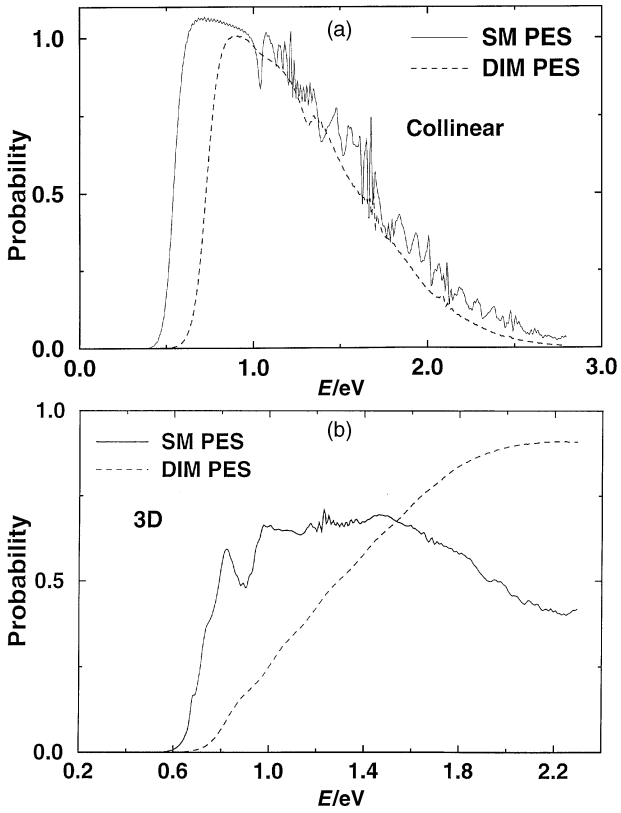

Fig. 4 Total reaction probability as a function of the total energy E for (a) collinear $H^- + H_2(v = 0) \rightarrow H_2(\Sigma v') + H^-$ and (b) three-dimensional ($J = 0$) $H^- + H_2(v = 0, j = 0) \rightarrow H_2(\Sigma v', \Sigma j') + H^-$ exchange reactions. The reaction probabilities obtained on the SM and the DIM potential energy surfaces are indicated by the solid and dashed lines, respectively.

with the dynamical features of the neutral reaction (R2). Additional work is presently in progress in order to have a detailed comparison between theory and experiment. We also note that the *ab initio* points are computed on a relatively coarse ($12 \times 8 \times 4$) grid in (R, r, γ) space by Stärck and Meyer. The grid along R extends from 2.4 a_0 to 13.5 a_0, the extension along r is from 1.0 a_0 to 2.4 a_0 and the angle γ is sampled at 0°, 30°, 60° and 90°.[17] Although their analytic fit to the *ab initio* data describes various stationary points of the PES accurately,[17] a more accurate description of the full potential energy hypersurface would probably need additional points along r (particularly for $r > 2$ a_0) and γ to be computed and incorporated into the functional fit.

IV. Summary

The initial ro-vibrational state selected and energy resolved total reaction probabilities of (R1) are reported on the DIM PES. The probabilities are obtained by the time–energy transformation of the reactive flux calculated with the aid of a three-dimensional time-dependent WP propagation method for the total angular momentum $J = 0$. The energetic threshold of the reaction (R3) occurs at $\sim$0.41 eV which compares well with the experimental results. The reaction probability of (R1) starting from the threshold reaches to a maximum value around $\sim$2 eV (for $v = 0, j = 0$) and then falls off at higher energies. This is analogous to the variation of the initial state selected cross section of (R3) for $v = 0, j = 0$ with energy, measured by Zimmer and Linder.[13] The reaction cross section starting from the threshold at $\sim$ 0.42 eV rises to a maximum around $\sim$1.5 eV and then decreases again.

A direct comparison between the theory and experiment can be made only when the reaction cross sections and the canonical or microcanonical rate constants are calculated. Such a study involves calculation of reaction probabilities beyond $J = 0$. We note that for the present, relatively simple, activated process the reaction probabilities for $J \neq 0$ can also be estimated from those for $J = 0$ by utilizing the J-shifting approach.[41] Such studies are presently in progress.

The qualitative variation of the reaction probability of (R1) with energy is similar to that found for the neutral reaction (R2). In contrast to that of (R2) the reaction probability curves of (R1) reveal more oscillations. The initial vibrational excitation of the reagent H_2 has been found to decrease the reaction probability (R1) at low and moderate energies. At high energies the reaction probability curves for different initial vibrational states of H_2 approach each other. We note that the reaction probability at high energies is expected to decrease further when the competing electron detachment process is taken into account. The energetic threshold of the reaction shifts to higher energy on vibrational excitation of the reagent H_2. A careful analysis revealed that only a fraction of the reagent vibrational energy is utilized to overcome the reaction barrier. The reagent translational energy is more efficient in promoting the reaction at low and moderate energies. With reagent rotational excitation the reaction probability increases much more rapidly at low energies and also decreases more rapidly at high energies. The effect is similar for all $j \neq 0$ states of the reagent H_2. Therefore, different orientation of the reagent molecule has a similar influence on the reaction. Interestingly, the existence of sharp resonances near the threshold is indicated in reactions with the ro-vibrationally excited reagent molecule. This is more clearly seen in the reaction probability curves for $v = 2$, $j = 0$–3 which exhibit severe oscillations near the reaction threshold.

The reaction probabilities of (R1) on the SM and the DIM potential energy surfaces exhibit a similar qualitative variation with energy. However, oscillations found in the reaction probability curves on the SM PES are absent in those on the DIM PES, both in the collinear ($v = 0$) as well as in the three-dimensional ($v = 0, j = 0$) results. As noted above the SM PES is the only *ab initio* PES available on the system and it is expected to describe the dynamics more accurately. Sensitivity of the results to the dividing surface position on this PES suggests more *ab initio* points are needed to have a smooth analytical representation of the PES. Therefore, it is felt that an accurate description of the global potential energy hypersurface for the ground electronic state of H_3^- is still necessary in order to have a detailed understanding of the dynamics of (R1) and to complement the experimental results satisfactorily. Although the reaction (R1) shares many features with its neutral analogue (R2), mechanistically they are very different. Therefore, having understood the reaction dynamics of (R2) in great detail both theoretically and experimentally, more theoretical work would be worth undertaking in order to understand the dynamics of the prototypical hydrogen exchange reaction (R1) involving a negative ion.

Acknowledgements

I am thankful to Professor A. K. Belyaev for providing me with the DIM PES of H_3^-. I am indebted to Professors N. Sathyamurthy, H. Köppel and L. S. Cederbaum for their interest in this work, encouragement and support.

References

1 (*a*) H. Buchenau, J. P. Toennies, J. Arnold and J. Wolfrum, *Ber. Bunsenges. Phys. Chem.*, 1990, **94**, 1231; (*b*) W. H. Miller, *Annu. Rev. Phys. Chem.*, 1990, **41**, 245; (*c*) G. C. Schatz, *J. Phys. Chem.*, 1996, **100**, 12839.
2 (*a*) P. Siegbahn and B. Liu, *J. Chem. Phys.*, 1978, **68**, 2466; (*b*) D. G. Truhlar and C. J. Horowitz, *J. Chem. Phys.*, 1978, **68**, 2466; (*c*) A. J. C. Varandas, F. B. Brown, C. A. Mead, D. G. Truhlar and N. C. Blais, *J. Chem. Phys.*, 1987, **86**, 6258; (*d*) A. I. Boothroyd, W. J. Keogh, P. G. Martin and M. R. Peterson, *J. Chem. Phys.*, 1996, **104**, 7139.
3 (*a*) L. Schnieder, K. Seehamp-Rahn, J. Borkowski, E. Wrede, K. H. Welge, F. J. Aoiz, L. Bañares, M. J. D'Mello, V. J. Herrero, V. Sáez Rábanos and R. E. Wyatt, *Science*, 1995, **269**, 207; (*b*) E. Wrede, L. Schnieder, K. H. Welge, F. J. Aoiz, L. Bañares, B. Martinez-Haya and V. J. Herrero, *J. Chem. Phys.*, 1999, **110**, 9971.
4 S. Mahapatra and H. Köppel, *Phys. Rev. Lett.*, 1998, **81**, 3116.
5 D. Stevenson and J. Hirschfelder, *J. Chem. Phys.*, 1937, **5**, 933.
6 (*a*) R. S. Barker, H. Eyring, D. A. Barker and C. J. Thorne, *J. Chem. Phys.*, 1995, **23**, 1381; (*b*) H. C. Bowen and J. W. Linnett, *Trans. Faraday Soc.*, 1964, **39**, 1186; (*c*) A. Macias, *J. Chem. Phys.*, 1968, **48**, 3464; (*d*) A. Macias, *J. Chem. Phys.*, 1968, **49**, 2198; (*e*) C. D. Ritchie and H. F. King, *J. Am. Chem. Soc.*, 1968, **90**, 825; (*f*) F. Keil and R. Ahlrichs, *J. Am. Chem. Soc.*, 1976, **98**, 4787; (*g*) J. C. Rayez, M. T. Rayez-Meaume and L. J. Maasa, *J. Chem. Phys.*, 1981, **75**, 5393.
7 H. H. Michaels and J. F. Paulson, in *Potential energy surfaces and dynamics calculations*, ed. D. G. Truhlar, Plenum, New York, 1981, p. 535; H. H. Michaels and J. A. Montgomery, Jr., *Chem. Phys. Lett.*, 1987, **139**, 535.
8 G. Chalasinski, R. A. Kendall and J. Simons, *J. Phys. Chem.*, 1987, **91**, 6151.
9 O. K. Kabbaj, F. Volatron and J. -P. Malrieu, *Chem. Phys. Lett.*, 1988, **147**, 353.
10 (*a*) E. E. Muschlitz, Jr., T. L. Bailey and J. H. Simons, *J. Chem Phys.*, 1956, **24**, 1202; (*b*) E. E. Muschlitz, Jr., T. L. Bailey and J. H. Simons, 1957, **26**, 711; (*c*) E. A. Mason and J. T. Vanderslice, *J. Chem. Phys.*, 1958, **28**, 1070.
11 (*a*) U. Hege and F. Linder, *Z. Phys. A*, 1985, **320**, 95; (*b*) H. Müller, M. Zimmer and F. Linder, *J. Phys. B*, 1996, **29**, 4165.
12 M. S. Haq, L. D. Doverspike and R. L. Champion, *Phys. Rev. A*, 1982, **27**, 2831.
13 (*a*) M. Zimmer and F. Linder, *Chem. Phys. Lett.*, 1992, **195**, 153; (*b*) M. Zimmer and F. Linder, *J. Phys. B*, 1995, **28**, 2671.
14 E. Haufler, S. Schlemmer and D. Gerlich, *J. Phys. Chem. A*, 1997, **101**, 6441.
15 A. K. Belyaev, D. T. Colbert, G. C. Groenenboom and W. H. Miller, *Chem. Phys. Lett.*, 1993, **209**, 309.

16 A. K. Belyaev and A. S. Tiukanov, *Chem. Phys.*, 1997, **220**, 43; A. K. Belyaev and A. S. Tiukanov, *Chem. Phys. Lett.*, in press.
17 J. W. Stärck and W. Meyer, *Chem. Phys.*, 1993, **176**, 83.
18 S. Mahapatra and N. Sathyamurthy, *J. Phys. Chem.*, 1996, **100**, 2759.
19 S. Mahapatra and N. Sathyamurthy, *Faraday Discuss.*, 1998, **110**, 228.
20 S. Mahapatra, N. Sathyamurthy, S. Kumar and F. A. Gianturco, *Chem. Phys. Lett.*, 1995, **241**, 223.
21 W. H. Ansari and N. Sathyamurthy, *Chem. Phys. Lett.*, 1998, **289**, 487.
22 (*a*) F. A. Gianturco and S. Kumar, *J. Chem. Phys.*, 1995, **103**, 2940; (*b*) F. A. Gianturco and S. Kumar, *J. Phys. Chem.*, 1995, **99**, 15342.
23 J. Tennyson and B. T. Sutcliffe, *J. Chem. Phys.*, 1982, **77**, 4061.
24 (*a*) D. Neuhauser and M. Baer, *J. Phys. Chem.*, 1989, **93**, 2872; (*b*) D. Neuhauser and M. Baer, *J. Chem. Phys.*, 1989, **91**, 4651; (*c*) D. Neuhauser, M. Baer, R. S. Judson and D. J. Kouri, *Comput. Phys. Commun.*, 1991, **63**, 460.
25 (*a*) D. H. Zhang and J. Z. H. Zhang, *J. Chem. Phys.*, 1993, **99**, 5615; (*b*) D. H. Zhang and J. Z. H. Zhang, *J. Chem. Phys.*, 1994, **100**, 2697; (*c*) D. H. Zhang and J. Z. H. Zhang, *J. Chem. Phys.*, 1994, **100**, 5631; (*d*) D. H. Zhang and J. Z. H. Zhang, *J. Chem. Phys.*, 1994, **101**, 1146; (*e*) D. H. Zhang and J. Z. H. Zhang, *J. Chem. Phys.*, 1994, **101**, 3671.
26 N. Balakrishnan, C. Kalyanaraman and N. Sathyamurthy, *Phys. Rep.*, 1997, **280**, 79, and references therein.
27 S. Mahapatra and N. Sathyamurthy, *J. Chem. Phys.*, 1997, **107**, 6621.
28 M. D. Feit, J. A. Fleck, Jr. and A. Steiger, *J. Comput. Phys.*, 1982, **47**, 412.
29 D. Kosloff and R. Kosloff, *J. Comput. Phys.*, 1983, **52**, 35.
30 Z. Bačić and J. C. Light, *Ann. Rev. Phys. Chem.*, 1989, **40**, 469.
31 (*a*) F. Quéré and C. Leforestier, *J. Chem. Phys.*, 1990, **92**, 247; (*b*) C. Leforestier, *J. Chem. Phys.*, 1991, **94**, 6388.
32 G. C. Corey and D. Lemoine, *J. Chem. Phys.*, 1992, **97**, 4115.
33 A. R. Offer and G. G. Balint-Kurti, *J. Chem. Phys.*, 1994, **101**, 10416.
34 D. T. Colbert and W. H. Miller, *J. Chem. Phys.*, 1992, **96**, 1982.
35 W. H. Press, B. P. Flannery, S. A. Teukolsky and W. T. Vetterling, *Numerical Recipes: The Art of Scientific Computing*, Cambridge University Press, Cambridge, 1986, p. 125.
36 S. Mahapatra and N. Sathyamurthy, *J. Chem. Soc., Faraday Trans.*, 1997, **93**, 773.
37 J. Z. H. Jhang, D. J. Kouri, K. Haug, D. W. Schwenke, Y. Shima and D. G. Truhlar, *J. Chem. Phys.*, 1988, **88**, 2492.
38 I. Last, A. Baram, H. Szichman and M. Baer, *J. Phys. Chem.*, 1993, **97**, 7040.
39 A. Jäckle and H.-D. Meyer, *J. Chem. Phys.*, 1998, **109**, 2614.
40 A. Jäckle, M.-C. Heitz and H.-D. Meyer, *J. Chem. Phys.*, 1999, **110**, 241.
41 (*a*) Q. Sun, J. M. Bowman, G. C. Schatz and J. N. L. Connor, *J. Chem. Phys.*, 1990, **92**, 1677; (*b*) J. M. Bowman, *J. Phys. Chem.*, 1991, **95**, 4960.

Paper a907521f